

Anomalous vortex state of superconducting LuNi₂B₂C

A. N. Price, R. I. Miller, R. F. Kiefl, J. A. Chakhalian, S. R. Dunsiger,* and G. D. Morris*
 TRIUMF, Canadian Institute for Advanced Research and Department of Physics and Astronomy, University of British Columbia,
 Vancouver, BC, Canada V6T 1Z1

J. E. Sonier

Department of Physics, Simon Fraser University, Burnaby, BC, Canada V5A 1S6

P. C. Canfield

Ames Laboratory and Department of Physics and Astronomy, Iowa State University, Ames, Iowa 50011

(Received 5 August 2001; published 6 June 2002)

Muon spin rotation has been used to investigate the magnetic-field distribution in the vortex state of superconducting LuNi₂B₂C ($T_c \approx 16$ K). Data for the magnetic field range $0.06H_{c2} \lesssim H \lesssim 0.23H_{c2}$ are fitted to a nonlocal London model. The temperature dependence of the vortex core radius shows a clear Kramer-Pesch effect due to depopulation of bound states within the cores. Also, the penetration depth and core radius vary substantially with applied magnetic field, suggesting the presence of anomalous field-induced quasiparticles and vortex-vortex interactions.

DOI: 10.1103/PhysRevB.65.214520

PACS number(s): 74.60.-w, 74.70.Dd, 76.75.+i

The internal magnetic-field distribution is a sensitive probe of the vortex state of a superconductor and the underlying physics. In an isotropic *s*-wave superconductor, theory predicts the formation of a hexagonal lattice of magnetic vortices each carrying an elementary quantum of flux. The resulting field distribution is determined by the applied field H along with the fundamental length scales: the magnetic penetration depth λ and the coherence length ξ . Roughly speaking λ determines the decrease in local magnetic field between vortices, whereas ξ determines the maximum magnetic field at the vortex center and the radius r_0 of the vortex cores.

In a simple model, λ and r_0 do not depend strongly on magnetic field or temperature deep in the superconducting state ($T \ll T_c$ and $H \ll H_{c2}$), where there are few excitations. Surprisingly however, both λ and r_0 extracted from muon spin rotation (μ SR) data often vary substantially with temperature and field in this region of the phase diagram, indicating that a more detailed theory is required. For example, vortices can support localized bound states in the superconducting energy gap with an energy spacing on the order of Δ^2/E_F ,¹ where Δ is the superconducting gap and E_F is the Fermi energy. According to the predicted Kramer-Pesch effect,²⁻⁴ thermal depopulation of such states causes r_0 to decrease with temperature until $r_0 \sim 1/k_F$ in the quantum limit, where $k_B T$ falls below the lowest bound-state energy. Such vortex shrinking was recently observed in NbSe₂,^{5,6} although the effect was weaker than expected. In addition, experiments on NbSe₂ (Ref. 7) and YBa₂Cu₃O_{6+x} (Refs. 6 and 8) showed that the vortex core radius expands in low magnetic fields $H_{c1} < H \ll H_{c2}$. Supporting evidence for this effect comes from Scanning tunneling microscopy⁹ (STM) and heat-capacity measurements¹⁰ in NbSe₂, and can be explained by the transfer of quasiparticles between vortices, which increases with decreasing vortex lattice spacing.¹¹ However, the lower dimensionality in these materials implies that the vortices may wobble in low magnetic fields,

thereby affecting the magnetic field distribution and increasing the fitted value of the core radius. It is therefore important to carry out similar measurements on isotropic superconductors.

A third anomalous effect is that the effective λ in the vortex state increases with magnetic field.^{7,6,12,13} This is observed in several superconductors, but is largest for YBa₂Cu₃O_{6+x}, where one expects strong nonlinear and nonlocal effects arising from nodes in the superconducting gap function.¹⁴

In this paper we report μ SR measurements of the magnetic-field distribution in the vortex state of LuNi₂B₂C [$T_c = 16$ K, $H_{c2}(0) = 7$ T],¹⁵ a nonmagnetic member of the borocarbide family of superconductors. Unlike NbSe₂ and YBa₂Cu₃O_{6+x}, LuNi₂B₂C has nearly isotropic electronic properties.¹⁶ Data in the field range $0.4 \text{ T} \lesssim H \lesssim 1.6 \text{ T}$ are fitted in the time domain to a nonlocal London model for the magnetic-field distribution, assuming a square vortex lattice.^{17,18} We observe a strong field dependence of the core radius, similar to that seen in quasi-two-dimensional (2D) superconductors. Furthermore, the Kramer-Pesch effect in LuNi₂B₂C is almost identical to that of NbSe₂.

Muon spin rotation experiments on LuNi₂B₂C were performed on the M20 surface muon channel at TRIUMF using a conventional horizontal He-cooled cryostat. As described elsewhere,¹³ the implanted spin-polarized muons stop randomly on the length scale of the vortex lattice and precess at a rate proportional to the local magnetic field. The muon ensemble-averaged precession signal is thus a direct measure of the distribution $n(B)$ of local internal magnetic fields. High statistics runs were made with approximately 20×10^6 muon decay events. The sample was a single crystal with a 2-cm² surface area, grown from a Ni₂B flux and polycrystalline LuNi₂B₂C mixture.^{19,20}

Figure 1 shows the time evolution of the muon polarization measured in LuNi₂B₂C in a magnetic field of 1.2 T

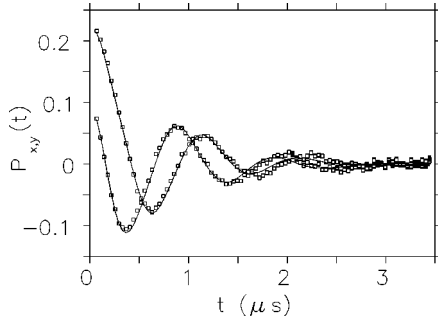


FIG. 1. The time dependence of the real and imaginary parts of the muon polarization signal $P(t) = P_x(t) + iP_y(t)$ in $\text{LuNi}_2\text{B}_2\text{C}$ in an applied field of $H = 1.2$ T at a temperature $T = 2.6$ K. The signal is displayed in a reference frame which rotates near the average Larmor frequency.

applied along the c axis. The rapid decay of the signal arises from the broad distribution of internal magnetic fields characteristic of the vortex state. The solid curves are a fit to a nonlocal London model developed for borocarbides to explain the magnetic-field-induced transition from a hexagonal to a square vortex lattice.^{17,21,22} In pure $\text{LuNi}_2\text{B}_2\text{C}$ the transition occurs in the region of 0.1 T, but shifts to higher magnetic fields in Co doped material.^{23,24}

For H parallel to the c axis, the nonlocal London model predicts a spatial dependence of the internal magnetic field $B(\mathbf{r})$ given by

$$B(\mathbf{r}) = \sum_{\mathbf{k}} \frac{\bar{B} \exp(i\mathbf{k} \cdot \mathbf{r}) \exp(-k^2 \xi^2 / 2)}{1 + \lambda^2 k^2 + \lambda^4 C (0.0705 k^4 + 0.675 k_x^2 k_y^2)}, \quad (1)$$

where \bar{B} is the average magnetic field, λ and ξ are the effective in-plane penetration depth and coherence length, respectively, and the \mathbf{k} 's are the reciprocal-lattice vectors of a square vortex lattice. The quartic and biquadratic terms in k are nonlocal corrections which scale with the fit parameter C . The quality of the fits was similar to that obtained for quasi-2D superconductors where a triangular vortex lattice is formed.¹³ Typically $\chi^2 \approx 800$ for about 550 degrees of freedom. We calculate the supercurrent density $J(r)$ from the fitted field profile $B(\mathbf{r})$, and extract the core radius r_0 , defined as the distance from the core center to the point in the nearest-neighbor core direction at which $J(\mathbf{r})$ is maximum.¹³ Core radii determined in this way are independent of the choice of model for $B(\mathbf{r})$, provided that the model fits the data well. It should be noted that changes to the model often produce a small shift in the absolute value of λ , but have much less influence on its temperature and field dependence.¹³

Figure 2 displays the real amplitudes of the Fourier transform of the measured polarization signal at two different temperatures in an applied magnetic field of $H = 1.2$ T. Such a transform approximates the internal magnetic field distribution $n(B)$ for an ideal vortex lattice, but is broadened by the finite-time window, flux lattice disorder, and random nuclear dipolar fields.¹³ Fits to the data in the time domain indicate that the latter two effects contribute a Gaussian broadening width σ which is much smaller than the width

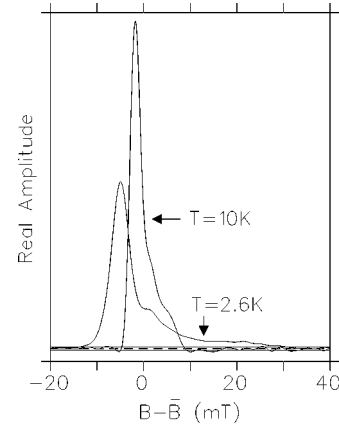


FIG. 2. Real amplitude of Fourier transforms of the measured polarization signal at $T = 10$ and 2.6 K. The dashed line represents zero amplitude, while the solid horizontal lines indicate the size of the ringing caused by transforming over a finite-time window.

due to the vortex lattice. For example, we find $\sigma = 1.1$ mT for the spectrum taken at 2.6 K. Near the average field \bar{B} in Fig. 2 is a small background peak, due to the small fraction ($\approx 5\%$) of muons which miss the sample. The shape of $n(B)$, as apparent from Fig. 2, evolves considerably with temperature. In particular the high-field tail is much more pronounced at 2.6 K, indicating that there is a significant Kramer-Pesch effect, as reflected by the decrease in the vortex core radius.

Figure 3 shows the temperature dependence of the fitted parameters and the extracted vortex core radius. The core radius [Fig. 3(a)] clearly decreases with temperature below $0.6T_c$. This is attributed to the Kramer-Pesch effect, where the shrinking of the cores is due to the depopulation of bound core states. STM measurements on $\text{LuNi}_2\text{B}_2\text{C}$ did not find evidence of bound core states, but this may be due to thermal broadening and the relatively small mean free path.²¹ The solid line in Fig. 3(a) is a fit of the $\text{LuNi}_2\text{B}_2\text{C}$ data, shown as solid circles, to the linear relation $r_0(T) = r_0(0)(1 + \alpha(T - T_0)/T_c)$ for $T > T_0$, with $\alpha = 0.84(5)$ and $T_0 = 1.0(4)$ K. In the fit $r_0(0)$ is set to 64 Å, since we expect a temperature-independent core radius in the quantum limit $T < T_0$, similar to that seen in NbSe_2 .⁵ For comparison, open circles depict the previous data on NbSe_2 . The slopes are almost identical, confirming that bound quasiparticle states play a similar role in the nearly isotropic $\text{LuNi}_2\text{B}_2\text{C}$ and quasi-2D NbSe_2 . The magnitude of the observed Kramer-Pesch effect is less than predicted by theories²⁻⁴ supposing static isolated vortices, which do not take into account zero point motion or interactions between vortices.¹³

Figure 3(b) shows the temperature dependence of the effective magnetic penetration depth. The curve is a fit to the BCS form with a single free parameter $\lambda(0) = 949(8)$ Å. Although the data are not sufficiently accurate to distinguish this form from a small linear term, the temperature dependence for $\text{LuNi}_2\text{B}_2\text{C}$ is definitely much weaker than that observed¹² in $\text{YBa}_2\text{Cu}_3\text{O}_{6.95}$, which has line nodes. Recent transport measurements¹⁵ at very low temperatures (70 mK) showed that the electronic thermal conductivity has a strong field dependence attributed to delocalized qua-

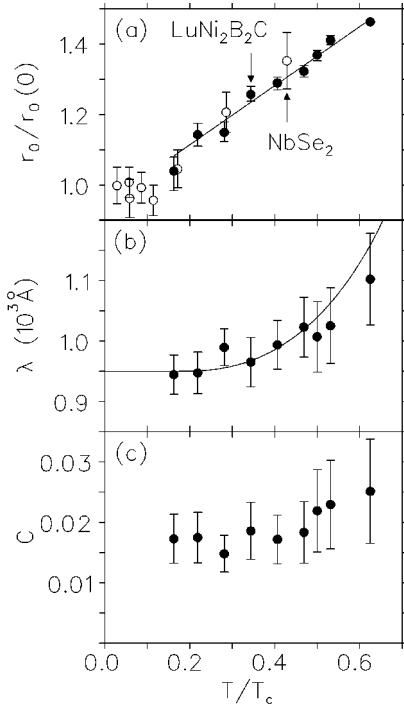


FIG. 3. Temperature dependence of the parameters used to fit the magnetic-field distribution in $\text{LuNi}_2\text{B}_2\text{C}$ in an applied magnetic field $H=1.2$ T. The solid circles in (a) are the current measurements of the vortex core radius, whereas the open circles are data for NbSe_2 from Miller *et al.* (Ref. 5) Panel (b) shows the effective magnetic penetration depth λ , while the curve is a fit to the BCS form. Panel (c) displays the nonlocal parameter C appearing in Eq. (1).

siparticles arising from a highly anisotropic gap function, possibly with nodes. The present result suggests that such excitations are not a strong function of temperature below about $0.5T_c$, although we also find evidence of substantial field-induced excitations (see below). Figure 3(c) shows that the nonlocal terms, as measured by C , are weak functions of temperature.

As shown in Fig. 4, the parameters r_0 , λ , and C all vary considerably with magnetic field. For example, the core radius r_0 in Fig. 4(a) increases at lower magnetic fields. This is similar to what is seen in the quasi-2D superconductors NbSe_2 ,⁷ $\text{YBa}_2\text{Cu}_3\text{O}_{6.60}$,⁶ and $\text{YBa}_2\text{Cu}_3\text{O}_{6.95}$.²⁵ Although vortices may not be well connected from plane to plane in quasi-2D materials, such a “vortex wobble” seems unlikely to influence the value of r_0 in nearly isotropic materials such as $\text{LuNi}_2\text{B}_2\text{C}$. Also, recent thermodynamic measurements on $\text{LuNi}_2\text{B}_2\text{C}$ showed that the Sommerfeld constant γ varies as $H^{0.63}$,²⁶ which is close to the predicted behavior for vortex expansion in *s*-wave superconductors.²⁷

Figure 4(b) shows that the penetration depth in $\text{LuNi}_2\text{B}_2\text{C}$ increases with applied field. This is similar to NbSe_2 ,⁷ $\text{YBa}_2\text{Cu}_3\text{O}_{6.95}$,¹² and $\text{YBa}_2\text{Cu}_3\text{O}_{6.60}$,⁶ where the increase is attributed to nonlinear and nonlocal effects. The field dependence of λ is expected to be larger in superconductors where the gap function has nodes or is very anisotropic.¹⁴ The solid line in Fig. 4(b) is a fit to the linear functional form $\lambda = \lambda_0(1 + \beta H/H_{c2})$, where $\lambda_0 = 590(20)$ Å and $\beta = 3.8(5)$.

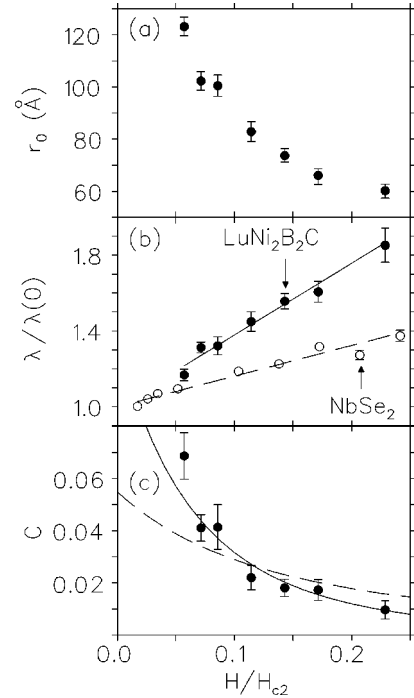


FIG. 4. The magnetic-field dependence of (a) the vortex core radius, (b) the effective magnetic penetration depth, and (c) the nonlocal parameter C in $\text{LuNi}_2\text{B}_2\text{C}$ at $T=2.5$ K. The parameters were obtained from fits to a nonlocal London model (see the text). In (b) the field dependence of λ is much stronger for $\text{LuNi}_2\text{B}_2\text{C}$ (solid circles) than for NbSe_2 (open circles). The dashed and solid curves in (c) are fits assuming C varies as $1/\lambda^2$ and $1/\lambda^4$, respectively.

For comparison, the dashed line and open circles are for NbSe_2 . The slope of $\lambda(H)$ for $\text{LuNi}_2\text{B}_2\text{C}$ is about twice that for NbSe_2 ($\beta=1.6$),⁷ and four times that reported recently for $\text{YNi}_2\text{B}_2\text{C}$ ($\beta=0.97$).²⁸ This strong field dependence appears in our effective λ even though the model includes first-order nonlocal corrections. This suggests that there are a significant number of field induced quasiparticles, which is consistent with the strong-field dependence seen in the low-temperature thermal conductivity,¹⁵ as well as theoretical work²⁹ arguing that $\text{LuNi}_2\text{B}_2\text{C}$ is a nodal superconductor. It is also possible that some of the field dependence we observe is due to the reduced accuracy of the London model in large magnetic fields.

The magnetic field dependence of the nonlocal parameter C [see Fig. 4(c)] is stronger than the theoretical prediction¹⁷ that C varies as $1/\lambda^2(H)$. If one takes our measured $\lambda(H)$ from Fig. 4(b), one would expect that C would fall off according to the dashed curve in Fig. 4(c). Assuming C varies as $1/\lambda^4(H)$ (solid curve) however, fits better empirically. The value for C extrapolated to the low field region is about a factor of 2 smaller than the estimate of 0.22 used to explain the vortex phase diagram at low fields.¹⁷ Our smaller C corresponds to weaker nonlocal effects and, therefore, a higher transition field $H_2(T)$ between the triangular and square vortex lattices. Indeed, a larger transition field $H_2(T)$ than that calculated for $C=0.22$ is observed through decoration images³⁰ and small-angle neutron scattering.³¹

In conclusion, we report μ SR measurements of the magnetic field distribution in the isotropic superconductor $\text{LuNi}_2\text{B}_2\text{C}$. A clear Kramer-Pesch effect is observed, due to thermal depopulation of bound quasiparticle states within the vortex cores. As with NbSe_2 , the effect is less than expected from theory for an isolated vortex. Additionally, the vortex core radius expands at low magnetic fields, as in some quasi-2D superconductors. Although the magnetic penetration depth λ shows a weak temperature dependence typical

of an energy gap at the Fermi surface, λ also shows a strong linear magnetic field dependence, which suggests a substantial number of field induced quasiparticles.

We gratefully acknowledge the help of Mel Good, Basam Hitti, Don Arseneau, and Syd Kreitzman, and the technical staff at TRIUMF. Ames Laboratory is operated for the U.S. D.O.E. by Iowa State University under Contract No. W-7405-Eng-82. This work was supported by the Director for Energy Research, Office of Basic Energy Sciences.

*Present address: Los Alamos National Laboratory, Los Alamos, New Mexico 87545

¹C. Caroli, P.G. de Gennes, and J. Matricon, *Phys. Lett.* **9**, 307 (1964).

²L. Kramer and W. Pesch, *Z. Phys.* **269**, 59 (1974).

³F. Gygi and M. Schlüter, *Phys. Rev. B* **43**, 7609 (1991).

⁴N. Hayashi, T. Isoshima, M. Ichioka, and K. Machida, *Phys. Rev. Lett.* **80**, 2921 (1998).

⁵R.I. Miller, R.F. Kiefl, J.H. Brewer, J. Chakhalian, S. Dunsiger, G.D. Morris, J.E. Sonier, and W.A. MacFarlane, *Phys. Rev. Lett.* **85**, 1540 (2000).

⁶J.E. Sonier, J.H. Brewer, R.F. Kiefl, D.A. Bonn, S.R. Dunsiger, W.N. Hardy, R. Liang, W.A. MacFarlane, R.I. Miller, T.M. Riseman, D.R. Noakes, C.E. Stronach, and M.F. White, Jr., *Phys. Rev. Lett.* **79**, 2875 (1997).

⁷J.E. Sonier, R.F. Kiefl, J.H. Brewer, J. Chakhalian, S.R. Dunsiger, W.A. MacFarlane, R.I. Miller, A. Wong, G.M. Luke, and J.W. Brill, *Phys. Rev. Lett.* **79**, 1742 (1997).

⁸J.E. Sonier, J.H. Brewer, R.F. Kiefl, G.D. Morris, R.I. Miller, D.A. Bonn, J. Chakhalian, R.H. Heffner, W.N. Hardy, and R. Liang, *Phys. Rev. Lett.* **83**, 4156 (1999).

⁹H.F. Hess, R.B. Robinson, R.C. Dynes, J.M. Valles, Jr., and J.V. Waszczak, *Phys. Rev. Lett.* **62**, 214 (1989).

¹⁰J.E. Sonier, M.F. Hundley, J.D. Thompson, and J.W. Brill, *Phys. Rev. Lett.* **82**, 4914 (1999).

¹¹M. Ichioka, A. Hasegawa, and K. Machida, *Phys. Rev. B* **59**, 8902 (1999).

¹²J.E. Sonier, R.F. Kiefl, J.H. Brewer, D.A. Bonn, S.R. Dunsiger, W.N. Hardy, R. Liang, W.A. MacFarlane, T.M. Riseman, D.R. Noakes, and C.E. Stronach, *Phys. Rev. B* **55**, 11 789 (1997).

¹³J.E. Sonier, J.H. Brewer, and R.F. Kiefl, *Rev. Mod. Phys.* **724**, 769 (2000).

¹⁴M.H.S. Amin, M. Franz, and I. Affleck, *Phys. Rev. Lett.* **84**, 5864 (2000).

¹⁵E. Boaknin, R.W. Hill, C. Proust, C. Lupien, L. Taillefer, and P.C. Canfield, *Phys. Rev. Lett.* **87**, 237001 (2001).

¹⁶I.R. Fisher, J.R. Cooper, and P.C. Canfield, *Phys. Rev. B* **56**, 10 820 (1997).

¹⁷V.G. Kogan, M. Bullock, B. Harmon, P. Miranovic, Lj. Dobrosavljevic-Grujic, P.L. Gammel, and D.J. Bishop, *Phys. Rev. B* **55**, R8693 (1997).

¹⁸I. Affleck, M. Franz, and M.H.S. Amin, *Phys. Rev. B* **55**, R704 (1997).

¹⁹P.C. Canfield, P.L. Gammel, and D.J. Bishop, *Phys. Today* **51** (10), 40 (1998).

²⁰X. Ming, P.C. Canfield, J.E. Ostenson, D.K. Finnemore, B.K. Cho, Z.R. Wang, and D.C. Johnston, *Physica C* **227**, 321 (1994).

²¹Y. DeWilde, M. Iavarone, U. Welp, V. Metlushko, A.E. Koshelev, I. Aranson, G.W. Crabtree, and P.C. Canfield, *Phys. Rev. Lett.* **78**, 4273 (1997).

²²M.R. Eskildsen, P.L. Gammel, B.P. Barber, A.P. Ramirez, D.J. Bishop, N.H. Andersen, K. Mortensen, C.A. Bolle, C.M. Lieber, and P.C. Canfield, *Phys. Rev. Lett.* **79**, 487 (1997).

²³P.L. Gammel, D.J. Bishop, M.R. Eskildsen, K. Mortensen, N.H. Andersen, I.R. Fisher, K.O. Cheon, P.C. Canfield, and V.G. Kogan, *Phys. Rev. Lett.* **82**, 4082 (1999).

²⁴K.O. Cheon, I.R. Fisher, V.G. Kogan, P.C. Canfield, P. Miranovic, and P.L. Gammel, *Phys. Rev. B* **58**, 6463 (1998).

²⁵J.E. Sonier, R.F. Kiefl, J.H. Brewer, D.A. Bonn, S.R. Dunsiger, W.N. Hardy, R. Liang, R.I. Miller, D.R. Noakes, and C.E. Stronach, *Phys. Rev. B* **59**, R729 (1999).

²⁶G.M. Schmiedeshoff, J.A. Detwiler, W.P. Beyermann, A.H. Lacerda, P.C. Canfield, and J.L. Smith, *Phys. Rev. B* **63**, 134519 (2001).

²⁷M. Ichioka, A. Hasegawa, and K. Machida, *Phys. Rev. B* **59**, 184 (1999).

²⁸K. Ohishi, K. Kakuta, J. Akimitsu, W. Higemoto, R. Kadono, A. N. Price, R.I. Miller, J.E. Sonier, R.F. Kiefl, M. Nohara, H. Suzuki, and H. Takagi, *Phys. Rev. B* **65**, 140505(R) (2002).

²⁹K. Maki, P. Thalmeier, and H. Won, *Phys. Rev. B* **65**, 140502(R) (2002).

³⁰L.Ya. Vinnikov, T.L. Barkov, P.C. Canfield, S.L. Bud'ko, and V.G. Kogan, *Phys. Rev. B* **64**, 024504 (2001).

³¹M.R. Eskildsen, A.B. Abrahamsen, V.G. Kogan, P.L. Gammel, K. Mortensen, N.H. Andersen, and P.C. Canfield, *Phys. Rev. Lett.* **86**, 5148 (2001).